RESEARCH ARTICLE

Key Points:
- Multidisciplinary study provides a refined understanding of eruption dynamics
- New seismic-based approach allowing high-frequency estimate of the lava flux
- Estimate of the initial overpressure and the volume of the magma reservoir

Correspondence to:
C. Hibert,
hibert@ldeo.columbia.edu

Toward continuous quantification of lava extrusion rate: Results from the multidisciplinary analysis of the 2 January 2010 eruption of Piton de la Fournaise volcano, La Réunion

C. Hibert[1,2,3], A. Mangeney[1,4], M. Polacci[5], A. Di Muro[6], S. Vergniolle[1], V. Ferrazzini[6], A. Peltier[6], B. Taisne[7], M. Burton[8], T. Dewez[2], G. Grandjean[2], A. Dupont[6], T. Staudacher[6], F. Brenguier[9], P. Kowalski[6], P. Boissier[6], P. Catherine[6], and F. Lauret[6]

[1]Institut de Physique du Globe de Paris, Equipe Sismologie, CNRS-UMR 7154, Université Paris Diderot 7, Paris, France, [2]Bureau des Recherches Géologiques et Minières, RNSC/RMT, Orléans, France, [3]Now at Lamont-Doherty Earth Observatory, Columbia University, New York, New York, USA, [4]ANGE Team, INRIA, CETMEF, Laboratoire Jacque Louis Lions, Paris, France, [5]Istituto Nazionale di Geofisica e Vulcanologia, sezione di Pisa, Pisa, Italy, [6]Observatoire Volcanologique du Piton de la Fournaise, Institut de Physique du Globe de Paris, Sorbonne Paris-Cité, CNRS UMR-7154, Université Paris Diderot, Bourg Murat, France, [7]Nanyang Technological University, Earth Observatory of Singapore, Singapore, Singapore, [8]School of Earth, Atmospheric and Environmental Sciences, University of Manchester, Manchester, UK, [9]Institut des Sciences de la Terre, Université Grenoble Alpes, Grenoble, France
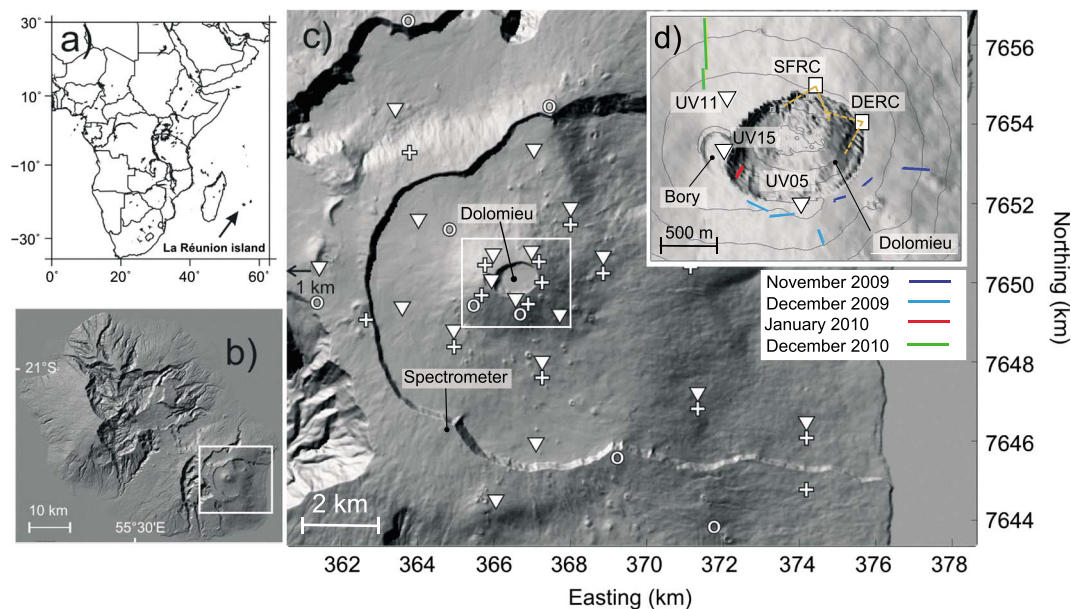
Abstract The dynamics of the 2–12 January 2010 effusive eruption at Piton de la Fournaise volcano were examined through seismic and infrasound records, time-lapse photography, SO_2 flux measurements, deformation data, and direct observations. Digital elevation models were constructed for four periods of the eruption, thus providing an assessment of the temporal evolution of the morphology, the volume and the extrusion rate of the lava flow. These data were compared to the continuous recording of the seismic and infrasonic waves, and a linear relationship was found between the seismic energy of the tremor and the lava extrusion rate. This relationship is supported by data from three other summit eruptions of Piton de la Fournaise and gives total volume and average lava extrusion rate in good agreement with previous studies. We can therefore provide an estimate of the lava extrusion rate for the January 2010 eruption with a very high temporal resolution. We found an average lava extrusion rate of 2.4 m^3 s^{-1} with a peak of 106.6 m^3 s^{-1} during the initial lava fountaining phase. We use the inferred average lava extrusion rate during the lava fountaining phase (30.23 m^3 s^{-1}) to estimate the value of the initial overpressure in the magma reservoir, which we found to range from 3.7×10^6 Pa to 5.9×10^6 Pa. Finally, based on the estimated initial overpressure, the volume of magma expelled during the lava fountaining phase and geodetic data, we inferred the volume of the magma reservoir using a simple Mogi model, between 0.25 km^3 and 0.54 km^3, which is in good agreement with previous studies.

1. Introduction

In the past few decades, a vast set of geophysical, geochemical, and geological approaches have been developed to understand the source processes of volcanic eruptions, to characterize volcano feeding systems, to determine the temporal evolution of eruptive activity, and to forecast eruptions. Recent technological advances, allowing wireless communication with monitoring stations and deployment of multisensor devices, provide increasingly broad access to large and complex data sets. Dense station networks are now commonly deployed on active volcanoes to monitor surface deformation, seismicity, degassing, thermal activity, and even the sound related to volcanic unrest. Gathering and comparing these data sets provides information that helps us to refine our understanding of the processes involved in initiating, sustaining, and terminating volcanic activity.

Piton de la Fournaise is a basaltic shield volcano forming the southeast part of La Réunion Island (Indian Ocean), 800 km east of Madagascar (Figure 1a). La Réunion is the youngest of the islands created by the Deccan Traps hotspot [*Duncan*, 1981]. Two main volcanic edifices form La Réunion Island : Piton des Neiges, which last erupted 12,000 years ago [*Deniel et al.*, 1992] and Piton de la Fournaise, which is still active, with

Figure 1. Location of (a) La Réunion Island, (b) Piton de la Fournaise volcano, and (c) the Undervolc and observatory seismic and GPS networks. Undervolc broadband seismic stations are shown as inverted triangles, GPS as crosses, and observatory short-period seismic stations as circles. This figure is in part a reproduction of *Brenguier et al.* [2012]. (d) Zoom on Piton de la Fournaise summit, showing the infrasonic station (UV15), the seismic station (UV11), and the photogrammetric stations (SFRC and DERC) used in this study. The fissure of the 2 January 2010 eruption is indicated in red. Eruptive fissures of the November and December 2009, and December 2010 eruptions are indicated by the corresponding colors in the legend.

an eruption every 8 months on average during the past 50 years [*Peltier et al.*, 2009; *Staudacher et al.*, 2009; *Roult et al.*, 2012]. The "Enclos Fouqué" caldera formed 4800 years ago and hosts the volcano's central summit cone [*Bachèlery*, 1981], and a small collapse of the volcano's summit occurred during the major 2007 flank eruption [*Michon et al.*, 2007; *Staudacher et al.*, 2009]. The majority of historical eruptions have occurred within Enclos Fouqué [e.g., *Staudacher et al.*, 2009; *Roult et al.*, 2012; *Michon et al.*, 2013]. Two main structures exist at the summit of the Piton de la Fournaise central cone: the Bory crater on the west, which is currently inactive, and the Dolomieu caldera on the east. The impressive collapse of the floor of the Dolomieu caldera in April 2007, with a drop of 340 m, occurred during the largest historical eruption of Piton de la Fournaise during which 210 Mm^3 of lava were emitted [*Staudacher et al.*, 2009; *Roult et al.*, 2012]. The caldera collapse was followed by a significant drop in extruded lava volumes and average lava flow rates in eruptions, which never exceeded 3 Mm^3 and 1 m^3 s^{-1}, respectively, during the 2008–2010 period [*Roult et al.*, 2012]. Most of the post-2007 eruptions have occurred at the top or close to the summit cone. This recent activity of Piton de la Fournaise is characterized by the arrival at the surface of a dyke fed by shallow magma reservoir located at about sea level [*Fukushima et al.*, 2005; *Peltier et al.*, 2007, 2008; *Prôno et al.*, 2009; *Massin et al.*, 2011]. Major eruptions like those of 1998 and 2007, in contrast, are associated with deeper seismicity and multiple magma sources [e.g., *Battaglia et al.*, 2005a; *Fontaine et al.*, 2014].

A permanent monitoring network, maintained by the Observatoire Volcanologique du Piton de la Fournaise/Institut de Physique du Globe de Paris (OVPF/IPGP), has been in place since 1980. The network consists of seismological and GPS stations, tiltmeters, extensometers, visible and IR cameras for direct monitoring, and a geochemical network (differential optical absorption spectroscopy (DOAS), MultiGaS, and CO$_2$ soil flux). Piton de la Fournaise eruptions have been extensively studied over the past decade. The permanent geophysical network was enlarged and densified in 2009 with stations deployed during the French (ANR) Undervolc project [*Brenguier et al.*, 2012]. Fifteen broadband seismometers with continuous GPS were installed and are now integrated into the permanent OVPF monitoring system (Figure 1c). Additionally, one infrasonic station was deployed in the Bory crater, directly overlooking the Dolomieu crater. The permanent geochemical network of DOAS sensors has been in operation since 2007 as part of the EU NOVAC project [*Galle*

et al., 2010]. Finally, two photogrammetric stations were deployed on the northern and eastern part of the Piton de la Fournaise summit for a direct monitoring of the southern inner part of Dolomieu crater (Figure 1d).

In this study we focus mainly on the January 2010 summit eruption, which is representative of the post-2007 Piton de la Fournaise activity and for which an unprecedented set of geophysical and geochemical data has been acquired. The eruption started at 10:20 (UTC) on 2 January 2010, on the southwestern inner wall of the Dolomieu caldera. As the eruption started during daytime on a clear day, the OVPF team could make direct observations of the early phase of the eruption. The eruptive fissure opened very close to the infrasonic sensor located in the Bory crater, and in direct sight of both photogrammetric stations located on the northern rim of the Dolomieu caldera (Figure 1d). Hence, in addition to the continuous monitoring (seismic, infrasound, GPS, and DOAS), this eruption was thoroughly documented by direct observations of surface processes, making it one the best documented eruptions at Piton de la Fournaise. The eruption lasted 10 days and ended at midnight on 11 January 2010. The volume of lava erupted is estimated from field observations to be 1.6 Mm^3 with an average lava extrusion rate of 2 m^3 s^{-1}.

Monitoring small-volume short-lived eruptions is highly challenging. The combined analysis of continuous data and direct observations can potentially provide insights into the dynamics of the eruption but also on the seismic and infrasonic signature of the different processes (degassing, lava fountaining, and steady lava flow). Furthermore, this approach can facilitate exploration into the quantitative relationships between the features of the continuous signals (amplitude, energy) and the volume and the extrusion rate of the lava flow.

In the first part of our study we provide a qualitative description of the timing and evolution of eruptive processes based on direct observations and photographs acquired in the field by the OVPF team. We then present the results of the lava flow reconstruction using photogrammetry monitoring, from which we were able to infer the lava extrusion rate. In section 3, we present the processing and the analysis of the continuous data recorded by the infrasonic and seismological stations. Section 4 focuses on the estimate of lava output rate on the basis of SO$_2$ degassing measured by UV DOAS spectrometry. In section 7, we discuss new insights into eruption dynamics provided by the combined analysis of the seismicity, lava extrusion rates inferred from photogrammetry, gas emissions, and direct observations of the eruption dynamics. Finally, based on these results and simple models, we infer the initial overpressure and the magma reservoir volume associated with the January 2010 eruption.

2. Timing and Dynamics of the January 2010 Eruption From Field Observations

A precursor seismic crisis was detected by the OVPF seismological network at 07:50 (UTC) on 2 January 2010 [*Taisne et al.*, 2011; *Roult et al.*, 2012]. The beginning of the eruptive tremor was recorded at 10:20 (UTC), indicating magma propagation and degassing very close to the surface, 2.5 h after the start of the seismic crisis. Observation from the western rim of Enclos Fouqué caldera (approximately 3 km from the central cone) identified a whitish gas cloud above Piton de la Fournaise summit at 10:27 (Figure 2a). At 10:56, the gas formed an approximately 1 km high vertical plume above the central cone (Figure 2b). The first direct observation of the Dolomieu caldera showed the presence of seven low-level lava fountains erupting from a fracture on the west Dolomieu caldera wall, with the highest fountain (30 m) located in the middle of the fracture (Figures 2c and 2d). The fountains ejected little fine ash, and a 5 cm thick bed of vesicular coarse lapilli scoria accumulated on the southern floor of Bory crater. The gas came out mainly from the large, middle vent and rose behind the low-level lava fountains (Figures 2c and 2e). Lava flows were fed both by magma extruded from vents and from fallback fountain products. Starting at 11:51, a series of rockfalls occurred on the caldera wall, close to the eruption site. The largest rockfall generated a block and ash flow and a convective "phoenix column" of fine material that rapidly dispersed in the atmosphere (Figures 2f to 2h).

Observations resumed at 3:58 on 3 January 2010. Only the largest central fountain was still active for the first hours of the day, with a maximum height of approximately 30 m (Figure 2j), and then progressively decreased to a height of 7 m prior to transitioning to energetic spattering. 'A'ā Lava had partially covered the caldera floor. The dark, cooled lava surface was cracked, and glow was observed in the flow interior.

On 4 January 2010, a complex lava flow field developed on the caldera wall, with different lava subbranches activating and stopping throughout the observation period (Figure 2k). Gas came out of the middle vent and from the fumaroles on the Dolomieu crater walls.

Figure 2. Chronology and dynamics of the 2–11 January 2010 Piton de la Fournaise eruption (UTC times): (a, b) gas plume over the Dolomieu crater; (c, d) eruptive fracture and lava fountaining during the first day of the eruption; (e–h) development of syneruptive rockfalls. Note the "phoenix" column from rockfall onto the lava flow in Figure 2f; (i) activity on second day of eruption (3 January 2010) with all lava fountains still active during the early hours of the day; (j) activity concentrates at the largest middle vent; activity during the (k) third (4 January 2010) and (l) fourth (5 January 2010) days of the eruption, which consisted of spattering at the only active vent and development of a complex lava field with lava tubes and secondary vents; (o) last day of the eruption (11 January 2010), when some weak degassing is still visible; and (p) Lava flow in the Dolomieu crater approximately 12 h after the eruption stopped.
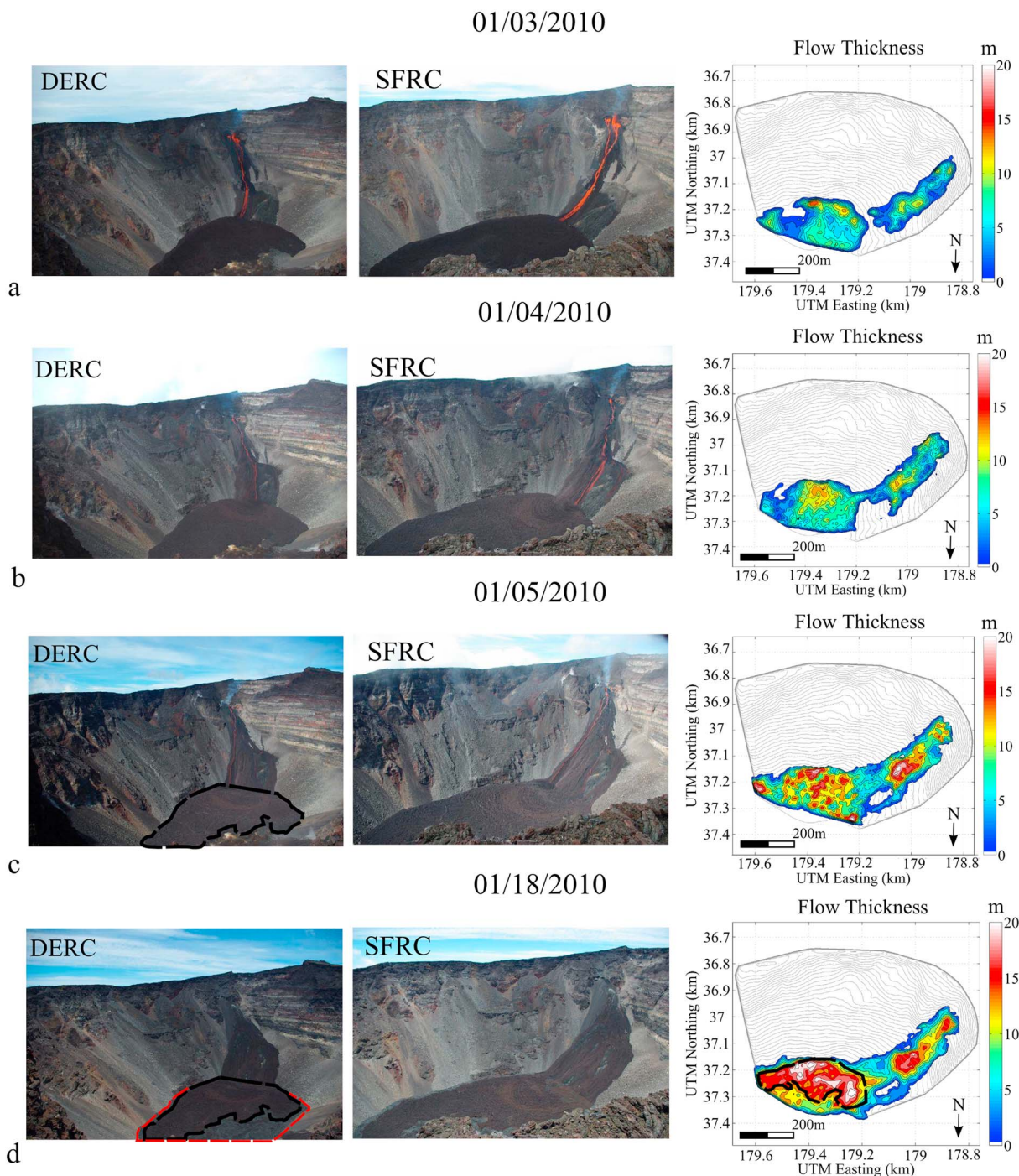
On 5 January 2010, spattering continued at the only active vent, which produced a weak gas plume. Lava flows came out of this vent with a dark, cooler central zone, likely associated to lower-temperature higher-viscosity lava. The fumaroles continued to degas. No lava fountains were observed (Figure 2l).

From 6 to 11 January, the lava flow field was still active, with lava running in tubes in the proximal part of the lava field, and with development of ephemeral vents in its central and distal areas (Figure 2m). During this period, 'a'ā lava had filled the bottom of the Dolomieu caldera. The active vent was mostly characterized by weak degassing (Figures 2n and 2o). On 11 January 2010, the seismic tremor started to decrease and reached background levels around midnight (UTC), indicating the end of the eruption after 10 days of activity. On 12 January 2010, no activity was visible at the surface (Figure 2p).

3. Photogrammetric Reconstruction of the Lava Flow Volume

Digital models obtained through aerial and land-based photogrammetry provide valuable information on the temporal evolution of the morphology of the lava flows, and, in general, on the continuous deformation of the

Figure 3. Photographs from the SFRC and DERC stations taken on (a) 3, (b) 4, (c) 5, and (d) 18 January 2010 and reconstructed DEM for these 4 days. The contour of the lava field observed on the 5 January 2010 is indicated by the black dashed line, and the final contour by the red dashed line on the photograph taken by DERC.

surface. Aerial- and ground-based photogrammetry and lidar have been used to reconstruct the morphology of lava flows to estimate their volume and thus the lava fluxes during Stromboli eruptions in 2002–2003 and 2007 [*Baldi et al.*, 2008; *Proietti et al.*, 2008]. These techniques were also used to assess the volume and rate of dome growth [*Major et al.*, 2009; *Diefenbach et al.*, 2012, 2013], which are critical factors for effective assessment of volcanic hazards related to potential dome collapses.

At Piton de la Fournaise, photogrammetry has been used to estimate the field of deformation related to the 1983–1984 eruptions [*Zlotnicki et al.*, 1990], which was then compared to a numerical model of the deformation induced by the dyke that fed the 1984 eruption [*Cayol and Cornet*, 1998]. Satellite imagery acquisition and aerial surveys are routinely performed at Piton de la Fournaise and provide information on a timescale ranging from a few days to months [e.g., *Coppola et al.*, 2009]. Those data provide an assessment of morphological changes and their association with output rates but do not permit high-resolution assessment of the rapid variability of eruptive dynamics during small-volume and short-lived eruptions. High-frequency (daily or less) photogrammetric surveys of an active lava flow are rare, however, due to the difficulty in installing devices in safe positions while providing a good view of the eruption.

A ground-based photogrammetric system at Piton de la Fournaise has been performing daily monitoring from the northeast flank of the Dolomieu caldera since mid-October 2009. It is comprised of two fully automatic photographic stations (modified Harbortronics Time-Lapse Package) equipped with Pentax K200D digital single-lens reflex cameras (18 mm lenses). The digital cameras from the off-the-shelf Harbortronics packages were connected to Asus EeePC 901 computers to download and broadcast daily photographs to the OVPF through its radio network. All the equipment is powered by solar panels and batteries. Cameras shot nine pairs of photographs per day, one every hour, from 08:00 to 16:00.

Stereopairs from the photogrammetric stations were used to assess the lava field thickness and morphology of the January 2010 eruption. Digital elevation models (DEMs) were constructed for 4 dates (3, 4, 5, and 18 January—Figure 3). Unfortunately, bad weather conditions made it impossible to compute and use DEMs for other days. The DEMs were constructed using PhotoModeler Scanner 6.0. Geometric errors introduced by the camera lens were previously calibrated in the laboratory using a calibration point grid. The point-based PhotoModeler project was chosen using these calibration parameters. Common points on photographs taken from both stations were manually identified and referenced.

For each day, we choose to compute DEMs in four steps with precision increasing from 30 m, to 10 m, then 5 m, and finally, 1 m, which is the expected final spatial resolution of our DEM. According to the information provided by the PhotoModeler software, the base-to-height ratio is 0.485, and the observation angle of our two stations is around 29°. This may not be optimal for very precise photogrammetric reconstruction, but field conditions (cracks, uneven topography) did not allow much choice in the location of the stations. The cameras provided photographs with a resolution of 3872 by 2592 pixels, their sensor size is 23.5 × 15.7 mm and their focal distance is 18 mm. The distance between the cameras and the caldera wall varies from 400 to 1000 m, resulting in a projected size of the pixels ranging from 14 to 34 cm.

The reconstructed morphology of the lava field and its temporal evolution match those observed from the photographs, with development of a subbranch on the caldera wall between 4 and 5 January and the widening of the main channel connecting the eruptive fissure to the spreading flow on the crater floor (Figure 3). This first lava channel does not appear on the first DEM (Figure 3a) because its thickness was too small in comparison with the resolution capability of the photogrammetry reconstruction, which was also complicated by the glowing texture of the surface of the active features, with the visible structure of the first lava field (marked by a dark line on the photograph taken by DERC station, Figure 3c) underneath which a second, grey lava appeared after 5 January 2010 (marked by a red line on DERC photograph, Figure 3d).

An estimate of the volume of the lava field was possible from the computed DEM. We infer the volume extruded for each period by computing the difference between a reference DEM constructed from photographs taken 1 day before the eruption and the reconstructed lava flow models. However, almost two fifths of the crater floor was not visible from our photogrammetric station, making it impossible to estimate the volume covering this area after 5 January 2010 (when lava flows advanced into this region). Hence, after this date we extrapolated the mean of the observed height of the lava flow to the unobserved surface when the lava flow reached this part of the crater floor, to make a rough estimate of the missing volume. The estimated total volume of lava erupted is 1.8 Mm^3 and the volumes inferred for each period are presented in Table 1. An uncertainty of 6% on the volume estimate has been determined from the quality of the point cloud given by PhotoModeler, surface comparison between ground truth and models, direct geodetic measurements and by taking into account the uncertainties caused by the extrapolation necessary after the 5 January 2010.

The lava extrusion rate was estimated for five eruptive stages. Our data suggest an overall decrease in lava extrusion rate over time. The highest lava extrusion rate of 9.5 m^3 s^{-1} occurred at the beginning of the eruption
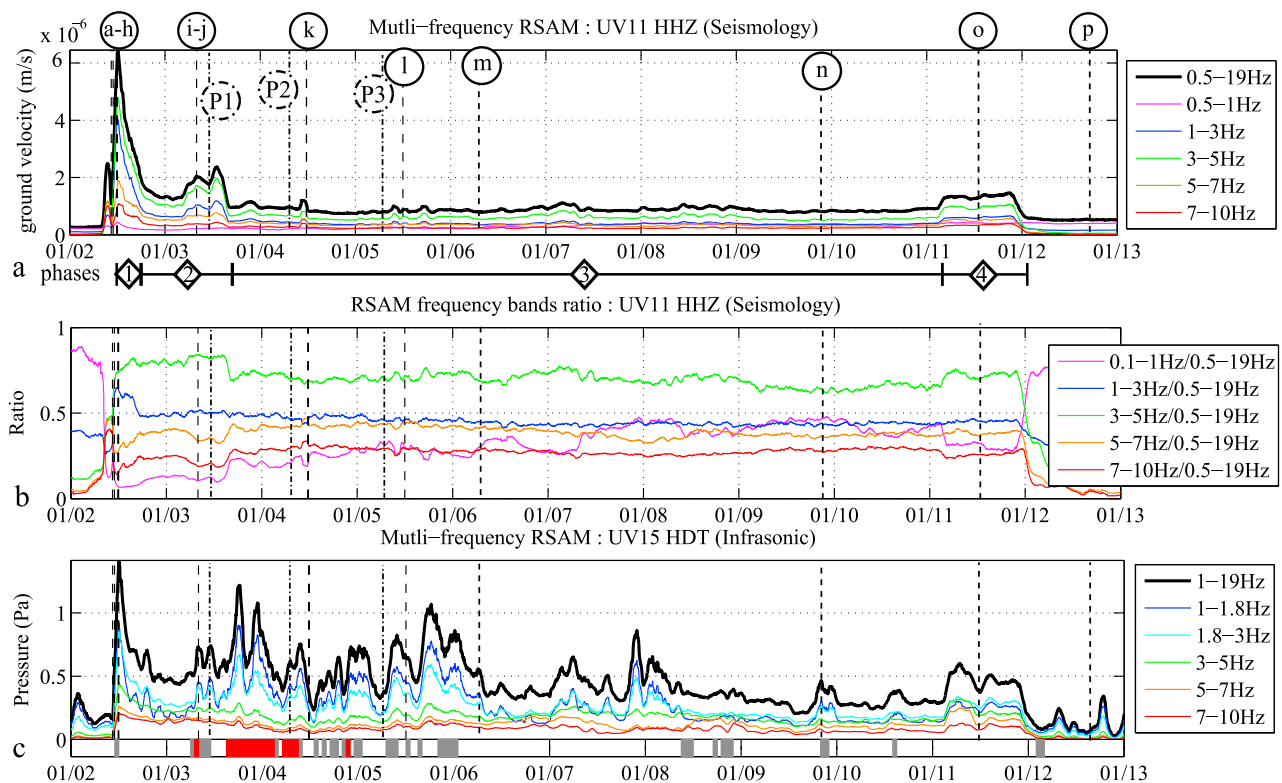
Table 1. Estimated Volumes and Corresponding Production Rate From the Computed DEM

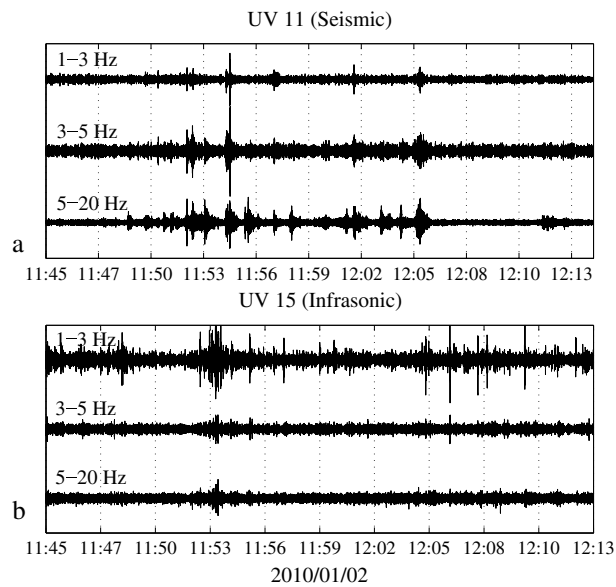| Day and Time (UTC + 4)	Estimated Volume (m^3)	Estimated Extrusion Rate (m^3 s^{-1})
2 January 2010 : 14:30	0	-
3 January 2010 : 08:00	0.6×10^6	9.5
4 January 2010 : 09:00	0.8×10^6	2.4
5 January 2010 : 08:00	1.2×10^6	4.8
12 January 2010 : 24:00	1.8×10^6	1.2

and was followed by a decrease of about 1 order of magnitude to 1.2 m^3 s^{-1} after 4 days of eruption. The average total extrusion rate was 2.4 m^3 s^{-1}, which is consistent with the average value of 1.5 m^3 s^{-1} estimated for similar eruptions that occurred within the Dolomieu crater by computing the ratio between their total volume over their total duration [*Peltier et al.*, 2007; *Roult et al.*, 2012].

4. Continuous Recording: Seismic and Infrasonic Data

Seismic activity was recorded at Piton de la Fournaise by the broadband seismometer array deployed for the Undervolc project and by the stations of the preexisting seismological network of the OVPF [*Brenguier et al.*, 2012]. We focused our study on the seismic signal recorded at the UV11 station (CMG40T 40 s, with a sampling rate of 100 Hz) installed north of Bory crater at a distance of approximately 400 m from the eruptive site. Infrasonic waves generated by the January 2010 eruption were recorded at an infrasonic station (microbarograph MB2005) located inside the Bory crater at a distance of about 100 m from the eruptive fissure. The sensor sensitivity was 20 mV/Pa and data were preprocessed by a 0.001–40 Hz band pass filtering.

Figure 4. (a) Smoothed RSAM computed with a 3 min time window on the vertical component of the UV11 station and for multiple frequency bands. Rounded letters indicate the time at which the corresponding pictures on Figure 2 were taken. P1, P2, and P3 indicate the times at which the photogrammetric pictures (Figure 3) were taken. The four different phases of the eruption are indicated below the *x* axis; (b) ratio of the smoothed RSAM signal filtered for six frequency bands over the RSAM computed for the 0.5 to 19 Hz frequency band; (c) smoothed RSAM computed with a 3 min time window on continuous infrasonic data recorded by the UV15 station, for multiple frequency bands. Periods when the infrasonic signal is dominated by the wind, identified by fast Fourier transform analysis, are indicated in red. During periods indicated in grey, wind perturbed the signal but volcanic activity dominates.
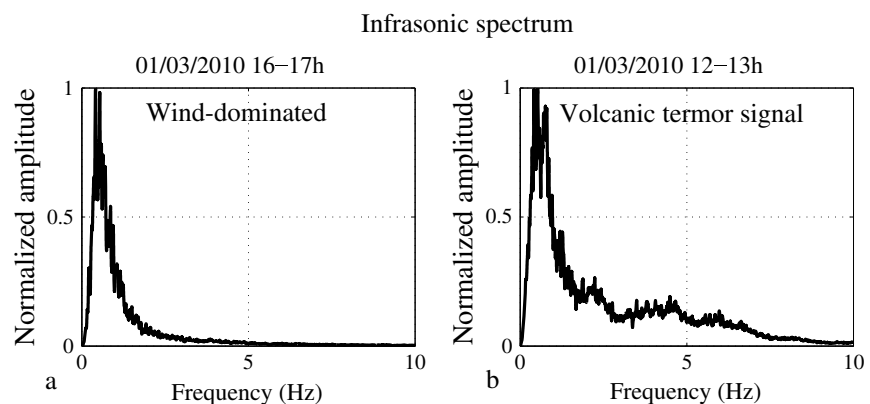
Figure 5. Seismic signals recorded at (a) UV11 seismic station and (b) UV15 infrasonic station during the sequence of rockfalls that occurred on 2 January 2010, between 11:50 and 12:06, normalized by the maximum amplitude of the raw signals and filtered in three frequency bands: 1–3 Hz, 3–5 Hz, and 5–20 Hz.

4.1. Multifrequency Infrasonic and Seismic Amplitude Measurement

Real-time Seismic Amplitude Measurement (RSAM) [*Endo and Murray*, 1991] was computed with a 3 min time window for 10 days of continuous data on the vertical component of the UV11 station, from 2 to 12 January 2010. The RSAM computation was done for six frequency bands where most of the seismic energy is observed for tremors at Piton de la Fournaise [*Aki and Ferrazzini*, 2000; *Battaglia et al.*, 2005a; *Staudacher et al.*, 2009]: 0.5–1, 1–3, 3–5, 5–7, 7–10, and 0.5–19 Hz (Figure 4a). The seismic signal in the frequency bands below 0.5 Hz was not included in our analysis as it was perturbed by the strong swell generated by cyclone Endazi occurring between 4 and 13 January 2010, approximately 1000 km away from La Réunion island. The ratios of each of these frequency bands over the 0.5–19 Hz band were also computed (Figure 4b). The equivalent of RSAM (3 min time window average amplitude measurements) was also computed for continuous infrasonic data recorded during the same period. The frequency bands chosen for the infrasonic processing were 1–1.8, 1.8–3, 3–5, 5–7, 7–10, and 1–19 Hz (Figure 4c), where most of the infrasonic signal energy is observed to be above wind level.

The RSAM computed for the seismic data and the equivalent time series for infrasonic data clearly show four different phases during the 2–12 January 2010 eruption:

1. The first phase starts with the beginning of the tremor on 2 January 2010 at 10:20 (UTC). This phase lasted approximately 8 h. The first 2 h were characterized by an increase in the seismic energy in the 1–3 Hz frequency band. The overall seismic signal is dominated by the 3–5 Hz frequency band and remained so until the end of the eruption. RSAM intensity quickly decreased during the hours following the initial 2 h increase in the seismic energy. The sequence of rockfalls observed on 2 January 2010 between 11:50 and 12:06 (Figures 2e to 2h) generated seismic signals clearly visible in the higher-frequency bands (Figure 5).

Figure 6. (a) Normalized frequency spectrum of infrasonic signal perturbed by strong wind; most of the energy is concentrated in a band centered on 1 Hz. (b) Normalized frequency spectrum of an infrasonic signal showing energy related to volcanic tremor in the 2–10 Hz band.

2. The second phase started on 2 January 2010 around 18:00 and was characterized by a high-amplitude tremor relative to the subsequent phases. This phase ended abruptly on 3 January, around 14:20, with a fast drop of the energy in the 3–5 Hz frequency band of the seismic signal. The second phase is not clearly defined in the infrasonic signal, which is probably related to noise generated by windy conditions, as discussed below.

3. The third phase starts on 3 January 2010 around 14:20 and was the longest but the least active phase, as shown by the low RSAM. It lasted approximately 8 days and ended on 11 January 2010 around 2:40. The seismic tremor exhibited only minor variations and was quite stable over the whole period. The infrasonic time series shows some amplitude variations, but these may not be related to the eruptive activity. Hour by hour analysis of the frequency spectrum of the infrasonic signals (using fast Fourier transform—Figure 6) makes it possible to identify periods during which the wind dominated over the signal generated by volcanic activity (Figure 6a—indicated in red on Figure 4c), and periods when wind perturbed the infrasonic signal but volcanic activity is still observable (indicated in grey on Figure 4c). Hence, we can see that most of the peaks observed at the beginning of phase 3 might be linked to windy conditions. Wind noise also prevented the use of the infrasonic signal filtered below 1 Hz, which may be more characteristic of the low-level lava fountains than frequencies above 1 Hz.

4. The last phase (phase four) started with a simultaneous sudden increase in the seismic and the infrasonic amplitudes on 11 January 2010 at around 2:40. The increase in the seismic amplitude is related to an increase in the energy in the 1–7 Hz frequency band. This phase is segmented in two parts in the infrasonic signal. A relative decrease in the energy in the 3–7 Hz band occurred during the second part that starts approximately at 12:00, while the energy in the 1–3 Hz remain at the same level. The volcanic tremor dropped to background levels at midnight (UTC), marking the end of the eruption.

4.2. Seismic and Infrasonic Energies

Several authors have demonstrated that seismic waves generated by volcanic tremor at some volcanoes (Masaya and Stromboli) are surface waves, consisting of Love and Rayleigh waves [*Métaxian et al.*, 1997; *Chouet et al.*, 1998] or only Rayleigh waves at Kīlauea volcano [*Ferrazzini et al.*, 1991]. At Piton de la Fournaise, *Aki and Ferrazzini* [2000] have also observed that volcanic tremor mainly consists of surface waves. A first approximation of the energy dissipated in the form of seismic surface waves between the times t_1 and t_2, assuming an isotropic homogeneous propagation medium, can be estimated with the equation [*Crampin*, 1965]:

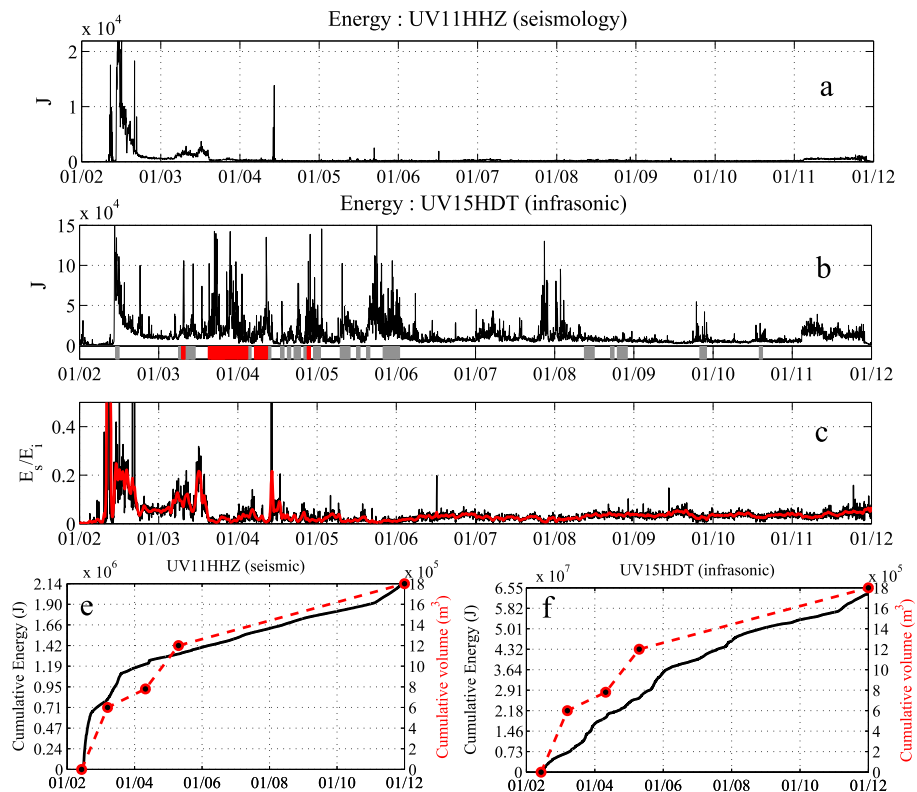$$E_s = \int_{t_1}^{t_2} 2\pi r \rho h c \, u_{\text{env}}(t)^2 e^{\beta r} \mathrm{d}t \tag{1}$$

with

$$u_{\text{env}}(t) = \sqrt{u(t)^2 + Ht(u(t))^2} \tag{2}$$

where r is the distance between the event and the recording station, ρ the density of the shallow layer in which the high-frequency surface waves propagate, h the thickness of this layer, and c the group velocity of the seismic waves. $u_{\text{env}}(t)$ is the amplitude of the envelope of the seismic signal (here the ground velocity) obtained using the Hilbert transform *(Ht)*, and β is a damping factor that accounts for inelastic attenuation of the waves [*Aki and Richards*, 1980]. This damping factor is frequency dependent and was computed as

$$\beta = \frac{f\pi}{Qc} \tag{3}$$

We choose a frequency $f = 3$ Hz, because this is the center of the 1–5 Hz frequency band where most of the energy is observed for the volcanic tremors [*Aki and Ferrazzini*, 2000; *Battaglia et al.*, 2005a; *Staudacher et al.*, 2009; this study]. On the basis of the typical phase velocity for surface waves in volcanic areas [*Ferrazzini et al.*, 1991; *Brenguier et al.*, 2007] and the significant fracturing of the upper layers of the caldera, we assume a velocity of $c = 1000 \text{ ms}^{-1}$ and a quality factor accounting for the attenuation of seismic wave $Q = 50$, which is within the range of the values obtained by *Aki and Ferrazzini* [2000] for surface waves generated by tremor

Figure 7. (a) Seismic energy and (b) infrasonic energy computed on 3 min moving windows for the whole eruption. Periods when the infrasonic signal is dominated by the wind, identified by fast Fourier transform analysis, are indicated in red. During periods indicated in grey, wind perturbed the signal but volcanic activity still dominates; (c) ratio of the seismic energy E_s over the infrasonic energy E_i (black) and corresponding smoothed curve (red); and comparison between the cumulative sum of the lava volume extruded estimated through photogrammetry (red) and (d) the cumulative sum of the seismic energy radiated and (e) the cumulative sum of the infrasonic energy radiated through the eruption (black).

observed at Piton de la Fournaise. The distance between the UV11 station and the eruptive vent is approximately $r = 400$ m. A thickness $h = 160$ m was taken as the wavelength of Rayleigh waves with a frequency peak of 3 Hz propagating with the velocity chosen. We assume a rock density of $\rho = 2000$ kg m^{-3} for the shallow fractured and weathered layers in which the high-frequency surface waves propagate. The seismic energy was calculated using a 3 min moving window on the seismic signal filtered between 1 and 5 Hz.

In the assumption of a compact infrasonic source radiating into a half-space from the surface, the energy of the degassing process produced at the source may be estimated from [*Pierce*, 1989]:

$$E_a = \frac{2\pi r^2}{\rho c} \int_0^T \Delta p^2(t)\mathrm{d}t \qquad (4)$$

where $r = 100$ m is the source-receiver distance, $\rho = 1.189$ kg m^{-3} is the air density at 2400 m above sea level, $c = 343$ m s^{-1} the atmospheric sound speed, and $\Delta p = p_{\text{inf}} - p_{\text{ambp}}$ is the fluctuation of the eruption infrasonic signal p_{inf} from the ambient pressure p_{ambp} as a function of time t, which is integrated over the signal duration T. We also computed the infrasonic energy on a 3 min moving window.

The four phases observed in the RSAM are also observed in the seismic energy time series (Figures 7a and 7b). The first phase is clearly the most energetic for both the infrasonic and the seismic signals. Few strong peaks are observed in the energy of the seismic signal, with the strongest occurring the 4 January at 10:00. Most of the strong energy peaks in the infrasonic signals observed between 3 and 6 January 2010 occurred during strong wind phases (Figure 7b) and are probably related to this noise. The whole eruption is dominated by the infrasonic energy, which is on average 5 times higher than the seismic energy during the first phase (Figure 7c). This ratio then decreases to 0.1 during the second phase and to an average value of 0.05 during the third and fourth phases.

The cumulative sum of each energy was computed and compared to the cumulative lava volume estimated from the photogrammetric results (Figures 7c and 7d). The cumulative seismic energy curve fits well with the cumulative lava volume curve, with a strong increase in energy production during the first phase of the eruption before reaching a stable regime. The cumulative infrasonic energy is less correlated with the cumulative lava volume and does not exhibit an initial strong increase but is rather constant. The potential nonvolcanic wind-related energy peaks observed between 3 and 6 January 2010 may have unduly influenced the trend of the cumulative infrasonic energy curve.

5. SO$_2$ Flux Estimate Through Spectrometry

Measuring the sulfur dioxide (SO$_2$) flux during an eruption can provide an estimate of the volume of magma extruded [e.g., *Allard et al.*, 1994; *Kazahaya et al.*, 1994; *Stoiber et al.*, 1986; *Sutton et al.*, 2001, 2003; *Harris et al.*, 2007]. *Sutton et al.* [2003] have shown that a good correlation exists at Kīlauea volcano between the lava extrusion rate and the discharge rates of SO$_2$. However, this correlation is good only if the degassing of the magma is synchronous with the extrusion. If the magma is degassed before reaching the surface, the lava extrusion rate will be underestimated [*Burton et al.*, 2005]. Conversely, an overestimate of the lava extrusion will occur if not all of the degassed magma is erupted [e.g., *Andres et al.*, 1991].

SO$_2$ emissions at Piton de la Fournaise are monitored by a network of three scanning ultraviolet (UV) spectrometers, distributed on the rim of the Enclos Fouqué caldera, installed as part of the EU NOVAC project. The main elements of these instruments are a scanning head connected optically via optic fiber cable to an Ocean Optics USB2000 spectrometer, controlled by a computer [*Galle et al.*, 2010]. Spectra are collected and processed before transmission to the observatory. Additional NOVAC software automatically calculates SO$_2$ fluxes. In January 2010, only one of the three spectrometers was running, located 3 km south southwest from the summit cone. Between 2 and 12 January 2010, wind switched daily from a southerly to a northerly direction with a relatively constant speed of 8.7 ± 4.9 km/h (courtesy of MeteoFrance,data measured 10 m above the ground at the Bellecombe meteorological station). At Piton de la Fournaise, SO$_2$ emissions are synchronous with eruptive or intrusive activity, as already reported by *Garofalo et al.* [2009], and drop below detection level during interruptive phases.

Unfortunately, the calculation of SO$_2$ flux from fixed scanners is not a trivial task. In order to produce robust, quantitative fluxes, knowledge of the plume geometry and plume height is needed. With a plume high above the instrument and well-constrained determinations of the wind velocity field, a good accuracy can be obtained even if the plume is observed with a single scanner. However, on Piton de la Fournaise, the network geometry is such that the SO$_2$ emissions may well be at low altitude over or even below the sensors. This makes quantitative determination of the SO$_2$ fluxes very challenging. Furthermore, the conversion of raw measured spectra to SO$_2$ column amount can be performed with a variety of approaches. In the standard NOVAC method, each spectrum in a scan, which consists of multiple UV spectra collected at different slant angles in an arc across the sky, is divided by the spectrum collected at zenith before proceeding with a standard DOAS retrieval procedure. This is done to remove artifacts and improves sensitivity to SO$_2$. However, if this zenith sky spectrum contains SO$_2$, which, in the case of an eruption at Piton de la Fournaise with a low plume is quite likely, then the amount of SO$_2$ in the 'clear-sky' spectrum will be removed from all the other spectra in the scan. This potential issue is partially resolved by offsetting the retrieved SO$_2$ profile to make the lowest value zero. This can produce issues, as when there is no gas present random noise can be offset to appear as a positive detection, or the flux can be significantly underestimated. We therefore applied a version of the approach used by *Salerno et al.* [2009] in which an artificial clear sky spectrum was used to normalize the measured scan spectra, thus avoiding issues with contaminated clear sky spectra.

Here we present SO$_2$ flux time series calculated using three different approaches: (i) with a constant average column height of 700 m for the whole eruption, (ii) with a column height exponentially decreasing in time from 1000 to 200 m above the central cone, and (iii) with the same decreasing rate but using the NOVAC spectral processing. Errors in plume height will lead to an overestimate of the SO$_2$ flux if the real plume is lower than the estimated height and an underestimate in the opposite case.

Flux of SO$_2$ released by the volcano is expressed in tons per day. The typical error on one flux measurement is approximately 35%. The first SO$_2$ detection above background values was at 10:34 (UTC), 7 min after the beginning of tremor on 2 January 2010. The highest SO$_2$ fluxes have been measured on 2 January 2010. Depending on the plume height considered and the method used, the peak value of SO$_2$ flux was between 1090 and

2580 t d^{-1} (Figure 8a). After 2 January 2010, SO$_2$ fluxes drop quickly below 400–600 t d^{-1}. At low SO$_2$ fluxes, the relative difference between SO$_2$ estimates increases slightly. NOVAC treatment tends to produce higher SO$_2$ flux estimates. The last SO$_2$ detection was at 12:44 on 11 January 2010, with an average SO$_2$ flux value of approximately 40–140 t d^{-1}.

The background SO$_2$ degassing rate at Piton de la Fournaise is effectively zero, and therefore, we can use these flux data as an indication of the erupted SO$_2$ flux. Using an estimate of the original SO$_2$ content of the magma obtained from petrological analyses as 0.174 wt % [*Di Muro et al.*, 2014], we may calculate the lava extrusion rate F required to produce the observed SO$_2$ fluxes F_{SO_2} by

$$F = \frac{10^3 F_{SO_2}}{0.864\,(C_{mi} - C_{gm})\,E_{psm}\,\rho_m} \tag{5}$$

With C_{mi} the SO$_2$ concentration in the melt inclusion in ppm, C_{gm} the residual SO$_2$ in the groundmass, E_{psm} the volume fraction of melt obtain from vesicularity data, and ρ_m the magma density for which we take a value of 2700 kg m^{-3}. Change in the magma density would proportionally impact the value of the inferred lava extrusion rate. Basaltic magma density typically ranges from 2600 kg m^{-3} to 2800 kg m^{-3} [e.g., *Murase and McBirney*, 1973] which, if taken into account in the lava extrusion rate computation, gives an uncertainty of ±3%. We assume an average magma vesicularity of 49 vol % similar to that observed in the natural samples [*Di Muro et al.*, 2014]. We used average C_{mi} = 2200 ppm and C_{gm} = 460 ppm values given by the petrological analysis presented in *Di Muro et al.* [2014].
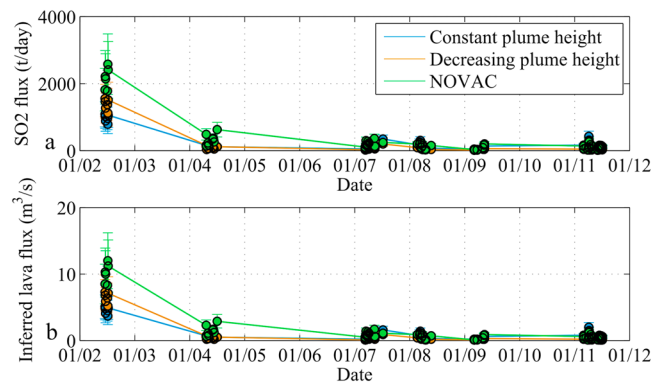
Maximum lava flux estimated with the three methods are 5.1 ± 1.8 m^3 s^{-1} with a constant plume height of 700 m, 7.3 ± 2.6 m^3 s^{-1} with an initial plume height of 1000 m, and 12.0 ± 4.2 m^3 s^{-1} with an initial plume height of 1000 m and the NOVAC processing (Figure 8b). The values obtained using a time-decreasing plume height bracket the photogrammetric estimate of 9.5 m^3 s^{-1}. Note that equation (5) is used to estimate lava flux by assuming that all sulfur is released by the melt during magma ascent and that other sources (e.g., deeper magmas, gas accumulation, and external fluids) do not play an important role. The good correlation obtained with the photogrammetric estimate of lava effusion rate suggests that most of the sulfur was released by ascending magma during the January 2010 eruption without a significant contribution from external sources.

6. Discussion From the Combined Analysis of the Different Methods
6.1. Eruption Dynamics From Analysis of Continuous Data and Direct Observations
Multifrequency time series computed for the infrasonic and seismic data show features that are apparently connected to the eruption dynamics described by direct observations. The multifrequency RSAM has shown that four phases can be distinguished during the January 2010 eruption (Figure 4). According to direct observations, the first seismic phase coincides with a set of complex events (magma ascent and degassing, vent opening). It was followed by a sustained lava fountaining activity, overlapping with rockfalls falling from the Bory cliff onto the lava flow. SO$_2$ analysis indicates that strong degassing existed during this phase, proportional to the higher initial lava extrusion rate. Photogrammetry measurements indicate high values for the lava extrusion rate during this first phase, which might be linked to an initially large fissure that focused on several vents and later transformed into a single vent as a result of thermal instability [*Bruce and Huppert*, 1989] after less than a day. As shown on Figure 5, sequences of rockfalls generated additional energy in the high-frequency bands of the seismic signals. Thus, rockfalls are probably not at the origin of the increase in the seismic energy in the 1–3 Hz frequency band of the RSAM observed during the first phase. The large width of the initial eruptive fissure may be responsible for the energetic low-frequency content of the seismic record, as previously suggested for seismic tremor [*Gordeev et al.*, 1990; *Benoit and McNutt*, 1997].

The low-level lava fountain was still observed during the second phase, but not at the beginning of the third. The transition between phases 2 and 3 occurred in less than 2 h and is marked by a drop in the energy of the seismic signal in the 3–5 Hz frequency band (Figure 4b). Hence, lava fountaining activity may generate a seismic signal dominated by energy in the 3–5 Hz band. This transition is also marked by a drop in the ratio between seismic tremor energy and infrasonic energy (Figure 7c). Infrasonic energy during Strombolian activity is mostly related to the breaking of large bubbles at the vent, hence to a separated two-phase flow [*Vergniolle and Brandeis*, 1996; *Vergniolle and Caplan-Auerbach*, 2004; *Vergniolle and Ripepe*, 2008], while the seismic energy might be related to magma motion [e.g., *Battaglia et al.*, 2005a]. Hence, the drop of the ratio between infrasonic and seismic energies may be interpreted as a fast transition between eruptive

Figure 8. (a) SO_2 flux estimate and (b) inferred lava flux obtained with a constant plume height of 700 m (blue), an exponential decrease in time of the plume height from 1000 m to 200 m (orange) and with the same decreasing rate in plume height model using NOVAC processing (green).
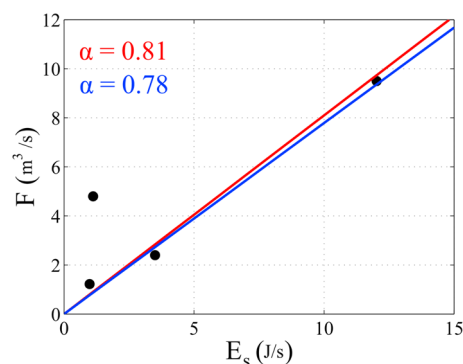
dynamics characterized by homogeneous magma flow, i.e., without bubbles or small stagnant bubbles, induced by the overpressure at the magma reservoir, to a two-phase flow mostly driven by degassing processes.

The beginning of the fourth phase is characterized by an increase in both the seismic and the infrasonic signal amplitudes but only very weak increase in SO_2 flux. Therefore, the increase in the infrasonic signal amplitude cannot be linked to the renewal of the passive degassing activity induced by the rise of the magma in the conduit. This observation is more likely to result from the enhanced and more energetic two-phase flow (slug type with bubbles as wide as the volcanic conduit).

6.2. Lava Extrusion Rate and Volcanic Tremor Seismic Energy

Seismic tremor amplitude is sometimes associated with the extrusion rate and effusive activity [*Aki et al.*, 1977; *Aki and Koyanagi*, 1981; *Ferrazzini and Aki*, 1992; *Coppola et al.*, 2009]. *Ferrazzini and Aki* [1992] have proposed that the seismic tremor is generated by the superposition of many gas-piston events. During the Pu'u 'Ō'ō eruption of Kīlauea volcano (Hawai'i), they observed that the burst of gas bubbles had an impact on the lava movement and was causing the vibration. More generally *Jaupart and Vergniolle* [1986, 1988] and *Vergniolle and Jaupart* [1990] have shown that degassing plays a major role in eruption dynamics. In this interpretation, the amplitude of the volcanic tremor would be directly correlated to the rate of burst and the size of the bubbles and hence to the lava extrusion rate if driven by the gas. This also implies that the infrasonic energy would be directly related to the lava extrusion rate.

Alternatively, seismic tremor could also be directly generated by magma flow inside the volcanic conduit and the associated friction on the conduit. In the simple case of the flow of a uniform incompressible viscous fluid in a cylindrical tube (Poiseuille flow), the dissipated energy is linearly proportional to the flux in the conduit [*Batchelor*, 1999]. Hence, in this interpretation, the lava extrusion rate would be linearly related to the seismic energy, which is computed from the squared amplitude of the tremor.

Battaglia et al. [2005b] have shown for the 1998–2000 eruptions of Piton de la Fournaise that the best estimates of the lava extrusion rate were obtained using the squared amplitude of the tremor filtered below 5 Hz, thus favoring the model of a seismic tremor generated by the friction of the magma flow on the conduit

Figure 9. Lava extrusion rate (F) as a function of the seismic energy (E_s) radiated per second by the volcanic tremor. The red line fits all the points while the blue line fits the three best aligned ones.

walls. Conversely, *Coppola et al.* [2009] have shown, using satellite remote sensing (Moderate Resolution Imaging Spectroradiometer), that the best correlation is found between the lava extrusion rate and the volcanic tremor amplitude for eruptions occurring during the 2003–2007 period, favoring the model of seismic tremor related to the rate of burst and the size of gas bubbles. The discrepancy between these results underlines the complexity and the diversity of eruptive processes that may exist at Piton de la Founraise volcano.

Our results show that the seismic energy release is well correlated to the extruded magma volume (Figure 7e), which is not the case for the infrasonic energy. This suggests that a linear relationship between seismic energy and lava extrusion rate exists for the January 2010 eruption, similar to what was observed by *Battaglia et al.* [2005b]. We computed the average seismic energy radiation per second over the periods for which photogrammetry made it possible to estimate the

Table 2. Volume and Average Flux Estimated From the Seismic Energy of the Tremor Recorded on UV05 and UV11 for Three Eruptions

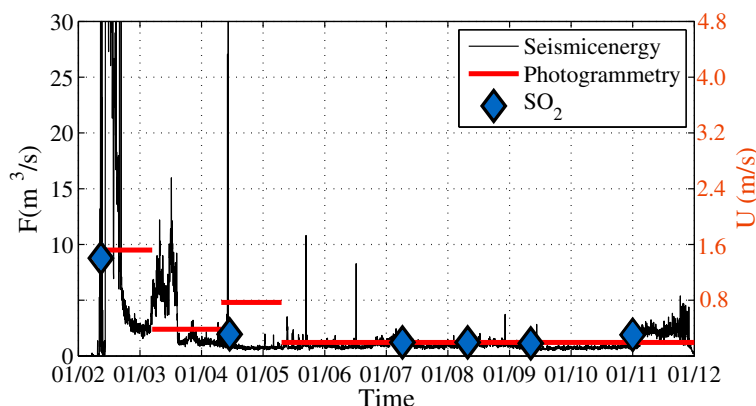| Eruption	Roult et al. [2012]		UV05 ($\alpha = 0.78$)		UV11 ($\alpha = 0.78$)		Best Factor α_{best}	
	V (Mm^3)	$\bar{F}$ (m^3 s^{-1})	V (Mm^3)	$\bar{F}$ (m^3 s^{-1})	V (Mm^3)	$\bar{F}$ (m^3 s^{-1})	UV05	UV11
2009/11/05	0.14	5.4	0.14	5.2	0.1	5.0	0.80	1.05
2009/12/14	0.16	2.3	0.13	2.3	0.16	2.7	0.94	0.80
2010/12/09	0.53	9.7	–	–	0.49	9.0	–	0.83

corresponding mean lava extrusion rate (Figure 9). Three of the four points align very well on a line that crosses the origin (blue line in Figure 9), suggesting that the lava extrusion rate (flux F) is proportional to the seismic energy radiated per second (E_s), as:

$$F = \alpha E_s \tag{6}$$

with $\alpha = 0.78$ (± 0.14 within 95% confidence interval; $R^2 = 0.99$). When trying to best fit the distribution of the four points by a line which crosses the origin (red line in Figure 9), the flux is then proportional to the seismic energy with $\alpha = 0.81$ (± 0.57 within 95% confidence interval; $R^2 = 0.61$).

To test the validity and assess the uncertainty made on the factor between the lava extrusion rate and the seismic energy of the tremor, we applied this relationship to eruptions that occurred on 5 November 2009, on 14 December 2009, and on 9 December 2010, close to the summit of Piton de la Fournaise. For each of these eruptions we computed the seismic energy of the tremor using equation (1) and the same seismological parameters (c, Q) as for the January 2010 eruption and by taking the topographical distance between the eruptive fissures and the UV05 and UV11 seismic stations. The lava extrusion rate and the total volume are inferred from the seismic energy of the tremor of the three eruptions, using the factor estimated for the January 2010 eruption ($\alpha = 0.78$). These values are compared to the average lava extrusion rate and the total lava volume given by *Roult et al.* [2012] (Table 2). The values given by *Roult et al.* [2012] for the total lava volumes were estimated via direct observations, and the average lava extrusion rates were obtain by dividing the total magma volume by the duration of the eruption, known precisely from seismic observations. The December 2010 eruption was far from the UV05 station and hence the seismic tremor amplitude was too weak to be included in our data set.

The total volume and the average lava extrusion rate inferred from the energy of the seismic tremor for the November 2009, December 2009, and December 2010 eruptions are in very good agreement with the values given by *Roult et al.* [2012], although slightly underestimated (Table 2). We computed, for the three eruptions and each station, adjusted ratios α_{best} that gives the exact values of the average lava extrusion rate and the total volume from the seismic energy (Table 2). The average value of these ratios is $\alpha_{best} = 0.87$ with a standard deviation of 0.11, equivalent to an uncertainty of about 13%. The uncertainty on the ratio comes from two distinct sources: (1) the values of the parameters used to compute the seismic energy in equation (1) are not

Figure 10. Lava extrusion rate F and magma ascent velocity U, considering a vent radius of 1 m, computed from the seismic energy (black) and compared to the values given by photogrammetry (red lines) and SO$_2$ emissions.

Table 3. Parameters Inferred From the Seismic Energy of the Different Eruptive Phases of the Four Summit Eruptions That Occurred in 2009 and 2010[a]
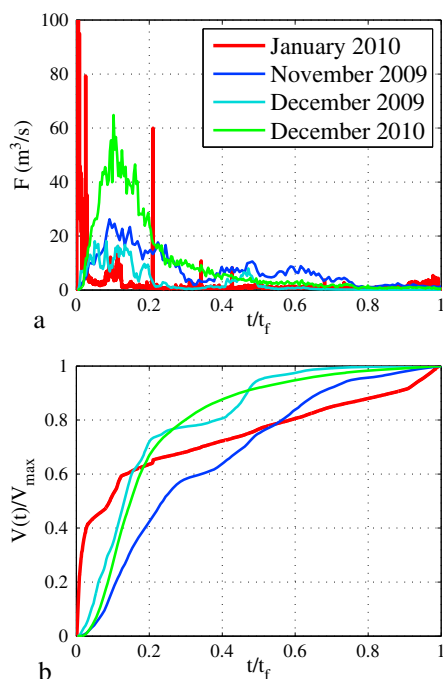
Eruption Phase	January 2010					November 2009			December 2009			December 2010
	1	2	3	4	Total	1	2	Total	1	2	Total	1
$\bar{F}$ (m³ s⁻¹)	30.2	4.6	1.0	2.2	2.4	13.4	2.9	5.2	9	0.6	2.5	9.0
F_{max} (m³ s⁻¹)	106.6	16.0	10.7	5.4	106.6	34.7	7.0	34.7	27.1	4.8	27.1	62.5
Volume (Mm³)	0.8	0.3	0.5	0.2	1.8	0.1	0.02	0.12	0.13	0.02	0.15	0.5
% Total volume	44%	17%	28%	11%	-	80%	20%	-	85%	15%	-	100%
Duration (h)	7.8	20.3	204.3	21.3	253.7	2.1	5	7.1	4.2	11.5	15.7	15

[a]For each phase we give the mean lava extrusion rate $\bar{F}$, the maximum lava extrusion rate F_{max}, the volume of lava extruded during this phase, the percentage of the extruded volume during this phase with respect to the total volume of lava emitted during the eruption, and the duration of the phase. Phase 1 is likely to be associated with the lava fountaining.

well known, especially the high spatial variability of the velocity of the surface waves within the shallow layers at the summit of Piton de la Fournaise [e.g., *Brenguier et al.*, 2012; *Hibert et al.*, 2014] and (2) the sources of tremor during usually move during eruptions, as eruptive fissures open and close, and the activity focuses at vents, which impact the computation of the seismic energy for which we assume a static point source. It is also important to note that the ratio α is dependent on the parameters used to compute the seismic energy. If, for example, the values of the density of the shallow layers or the velocity of the seismic waves used in equation (1) are set to be higher or lower than those we have chosen, the ratio α would increase or decrease accordingly. However, the correlation between the seismic energy and the lava extrusion rate would still exist.

From equation (6) and the coefficients α presented in Table 2 we can reconstruct the continuous evolution of the lava extrusion rate during the January 2010 eruption. The lava extrusion rate compared well with the values given by SO_2 and photogrammetry measurements, except for the third period during 4 to 5 January 2010 for which the photogrammetry gives higher values than that inferred from the seismic tremor energy (Figure 10). As shown in Figure 10, a very strong burst of seismic energy occurred on 4 January 2010 around 10:00 and might be related to high extrusion rate activity. Thus, as the photogrammetry estimates the lava volume extruded over a specific duration, if a very large proportion of this volume was extruded during a very brief time, this would lead to an overestimate of the mean lava extrusion rate for this period. This may explain the discrepancy we observed between the lava extrusion rates estimated through photogrammetry and the seismic tremor energy for this specific period.

For each eruption, using equation (6), we can also provide the maximum lava extrusion rate F_{max}, the mean lava extrusion rate $\bar{F}$, and the volume extruded during their distinct phases (Table 3). For the January 2010 eruption we computed those parameters for the four phases described previously and shown in Figure 4. For the other eruptions, we identify a first phase with a fast increase preceding a relatively slow decrease in seismic energy, followed by a second phase with an almost constant seismic tremor amplitude (Figures 11a and 11b). For the December 2010 eruption there is no second phase; the eruption stopped just after the fast decrease in the first seismic tremor peak. These parameters were computed from stations UV11 and UV05, when available, and averaged. We used, for each eruption and each station, the best coefficients α_{best} presented in Table 2.

Figure 11. (a) Lava extrusion rate and (b) normalized cumulative volume inferred from seismic energy for the January 2010, November 2009, December 2009, and December 2010 eruptions as a function of the normalized duration. Total duration t_f and maximum volume V_{max} are given in Table (3).

6.3. Initial Overpressure and Lava Extrusion Rate

Two types of flows are possible in the conduit, depending on whether viscous forces or inertial forces are dominant, called laminar flow and turbulent flow, respectively. The transition between the two regimes depends on the value of a dimensionless number, the Reynolds number Re, computed from the ratio between inertial and viscous forces by

$$Re = \frac{\rho_m \, U \, R_{cond}}{\mu} \qquad (7)$$

where ρ_m is the magma density, U the magma ascent velocity, R_{cond} the conduit radius, and μ the magma viscosity. Laminar flow exists for Reynolds numbers below 2300 for a smooth pipe [*White*, 1994], and the value for the transition from laminar to turbulent flow is classically taken to be 2000. The magma velocity U in the conduit ranges from 3 m s^{-1} to 0.4 m s^{-1} for a conduit radius R_{cond} estimated to be approximately 1 m from photogrammetric observation and a lava extrusion rate between 9.5 and 1.2 m^3 s^{-1}. Using the model proposed by *Giordano et al.* [2006] and taking an average temperature of the lava of 1150°C [*Staudacher*, 2010] and the composition of 2010 aphyric lavas [*Di Muro et al.*, 2014], we compute an average viscosity of 40 Pa s. Finally, by taking a classical value of 2700 kg m^{-3} for the magma density ρ_m, we estimate the Reynolds numbers Re to range from approximately 20 to 200. If we take into account the mean and maximum lava extrusion rate estimated from the seismic energy (Table 3) which are 30.2 m^3 s^{-1} and 106.6 m^3 s^{-1}, the Reynolds numbers Re ranges from 650 to 2100. The peak lava extrusion rate gives a Reynolds numbers Re slightly above the transition threshold but was sustained for a very short duration. Therefore, the lava flows extruded during the entire January 2010 eruption occurred in the laminar regime dominated by the viscous forces.

The flow rate at the vent is, for laminar (Poisseuille) flows occurring in a cylindrical conduit and produced by an initial overperssure ΔP [*White*, 1994; *Jaupart*, 2000] :

$$F = \frac{\Delta P \pi R^4_{cond}}{8 \mu L}, \qquad (8)$$

where ΔP is the initial overpressure (assumed to be constant), R_{cond} the conduit radius, μ the magma viscosity, and L the length of the conduit. Consequently, the initial overpressure is given by:

$$\Delta P = \frac{8 F \mu L}{\pi R^4_{cond}}, \qquad (9)$$

Taisne et al. [2011] have shown that migration of magma started from the shallow magma storage located near sea level, 2500 m below the summit of Piton de la Fournaise [*Nercessian et al.*, 1996; *Peltier et al.*, 2007; *Prôno et al.*, 2009]. GPS data inversion suggests that the roof of this reservoir is located at an altitude of about 800 m above sea level [*Peltier et al.*, 2008], and hence, the length of the conduit is approximately 1700 m.

To infer the overpressure, we first considered the lava extrusion rate given by photogrammetry measurements, which is averaged over the first phase and a large part of the second one. However, the second phase might be associated with a residual overpressure in the magma reservoir and not the initial overpressure, leading to an underestimate of the initial average lava extrusion rate and thus of the initial overpressure. We therefore have to estimate the average lava extrusion rate of the initial overpressurized phase only. The end of the initial overpressurized period is not straightforward to determine. Direct observations at 3:58 and 11:39 (Figures 2i and 2j) suggest that the 30 m high lava fountain was active at least until the morning of 3 January. However, the sudden drop in the ratio between seismic and infrasonic energy around 18:00 on the 2 January (end of phase 1), suggests that the overpressure in the magma reservoir, and the associated lava fountains, might have stopped at that time. In this case, the lava fountains observed at 3:58 and 11:39 on 3 January (Figure 2j), which also coincide with small peaks in the ratio between seismic and infrasonic energy, may have a different origin than the lava fountains of the first day, such as strong but sporadic active degassing.

By using the relationship between extrusion rate and seismic energy (equation (6)), we can estimate the average lava extrusion rate of phase 1 (Table 3), from the seismic energy of the volcanic tremor and using $\alpha = 0.78$ and an uncertainty of 13% on this ratio. We found an average lava extrusion rate for the first phase of approximately 30 ± 4 m^3 s^{-1} ($U = 9.5$ m s^{-1}; $Re = 650$), which, using equation (9), gives an initial overpressure value of $5.2 \pm 0.7 \times 10^6$ Pa, in the range of the values given by *Peltier et al.* [2008] for the pre-2007 period (Table 4).

Table 4. Inferred Reservoir Volume[a] for Eruptions During 2004–2006

	Peltier et al. [2008]		Volume Reservoir (Equation (11))
Eruption	ΔV (10^6 m^3)	ΔP (MPa)	V_{res} (10^9 m^3)
Aug.–Oct. 2004	0.58	4.7	0.55
Feb. 2005	0.41	3.4	0.53
Oct. 2005	0.55	4.3	0.57
Nov. 2005	0.65	5.2	0.55
Dec. 2005 to Jan. 2006	0.44	3.7	0.53

[a]Reservoir volume V_{res} inferred from equation (11) using initial overpressure ΔP and volume change ΔV in the reservoir obtained through geodetic measurements and given by *Peltier et al.* [2008] for five eruptions that occurred between August 2004 and January 2006.

6.4. Characteristics of the Shallow Feeding System Involved During the 2 January 2010 Eruption

The internal structure and the feeding system of Piton de la Fournaise volcano are complex and still not fully understood. Recent studies have shown that two zones might be connected and active during particular eruptive episodes. The first shallow zone is located at sea level, and geophysical monitoring shows that it is active during most of the eruptions at Piton de la Fournaise volcano [e.g., *Battaglia et al.*, 2005a; *Peltier et al.*, 2009; *Prôno et al.*, 2009; *Massin et al.*, 2011; *Taisne et al.*, 2011]. A second structure, located at approximately 2 km below sea level, might correspond to the principal magma chamber and is thought to be activated mainly during major eruptions, such as the March 1998 eruption [*Prôno et al.*, 2009] or the 2007 eruption [*Fontaine et al.*, 2014].

No deep seismicity was observed during the January 2010 eruption, and the location of the first volcano-tectonic earthquakes of the seismic crisis shows that the dyke must have started its propagation at approximately 1700 m below Piton de la Fournaise summit, at the top of the first structure described above. Hence, we assume the overpressure we inferred is that of the shallow magma storage structure, located at sea level. However, it is possible that the actual overpressure source is more extended, with a connection between the shallow and the deep structures before and during the eruption. Note that if we were to consider that the eruption sourced from the top of the magma reservoir located 2 km below sea level ($L = 3600$ m), the calculation of the overpressure from equation (9) can give the same overpressure value as the one we estimated, in agreement with GPS data and deformation modeling for the pre-2007 period [*Peltier et al.*, 2009], by only increasing the conduit radius R_{cond} by approximately 20%. This also highlights the very high sensitivity of the overpressure estimate to the radius of the conduit.

We have so far proposed that the large lava extrusion rate during the low-level lava fountains at Piton de la Fournaise is induced by the initial overpressure in the magma storage zone located at sea level, which pushes viscous magma upward in the conduit (equation (9)). Within this framework, we can also assume that the volume of magma expelled during the low-level lava fountain corresponds to an excess of volume accumulated in the structure located at sea level prior to the eruption.
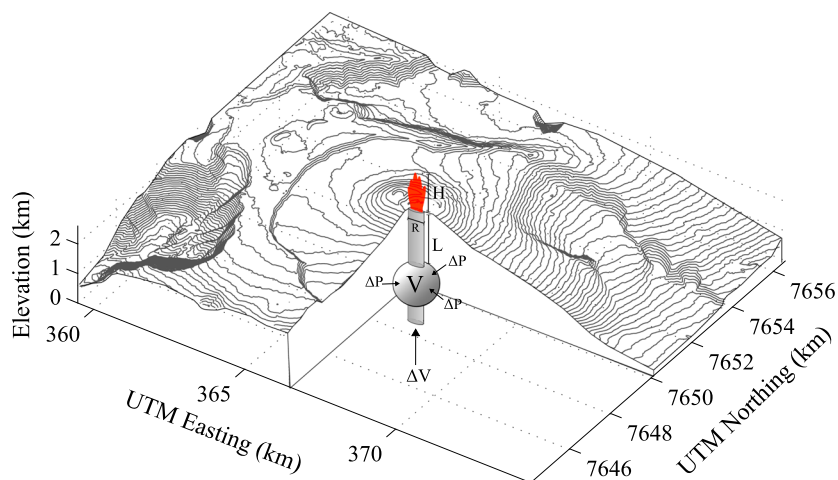
A rough estimate of the shallow magma reservoir volume can be inferred from a simple model which considers the reservoir to be a spherical source [*Mogi*, 1958] (Figure 12). In the absence of good constrains on magma compressibility and the density difference between the host rock and the magma for the post-2007 collapse period at Piton de la Fournaise volcano, we consider here the simplest model consisting of a homogeneous medium with incompressible magma. With these assumptions we have

$$\frac{\Delta V}{V_{res}} = \frac{3\Delta P}{4K}, \tag{10}$$

where ΔV is the volume change of the reservoir (due to new magma injection and/or gas exsolution), V_{res} the initial reservoir volume, ΔP the overpressure at the beginning of the eruption, and K the bulk modulus of the surrounding medium. The reservoir volume V_{res} is then given by

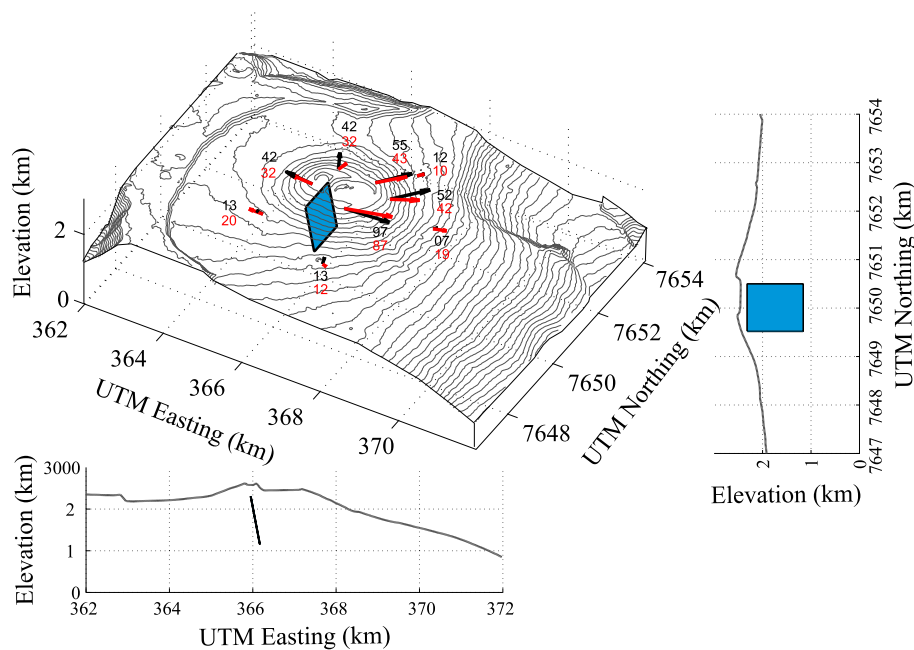$$V_{res} = \frac{4K\Delta V}{3\Delta P}, \tag{11}$$

Figure 12. Schematic representation of the simple Mogi source model and the parameters used to determine the volume of the magma reservoir that supplied the January 2010 eruption.

The volume of magma extruded until the end of the first phase, at 18:00 on the 2 January 2010, estimated from the relationship between extrusion rate and seismic energy (equation (6)) with $\alpha = 0.78$ and an uncertainty of 13%, is equal to approximately $0.8 \pm 0.1 \times 10^6$ m³. Considering the volume expansion related to gas bubbles formation and growth during the extrusion of the magma toward the surface, and an average vesicularity of 49 vol % [*Di Muro et al.*, 2014], we can assume that the volume of the aphyric melt released at the surface ΔV_{Surf} is approximately $0.4 \pm 0.05 \times 10^6$ m³ during this period.

The bulk modulus K is approximately 3.33 GPa, assuming that the volcanic edifice is elastic, homogeneous and isotropic, with a Young's modulus E=5 GPa and a Poisson's ratio $\nu = 0.25$ [*Cayol and Cornet*, 1998; *Peltier et al.*, 2008]. When assuming that the emitted volume at the surface ΔV_{Surf} during the initial overpressurized phase is roughly equal to the magma volume injected in the reservoir ΔV and by taking into account the uncertainty made on this estimate of the volume and on the initial overpressure, the inferred reservoir volume

Figure 13. Ground displacements recorded at the surface (black) and modeled (red) using by an Okada source model located beneath the central cone of the Piton de la Fournaise. Amplitude of the displacement is given in millimeters next to the corresponding arrow.

would be approximately 0.35 ± 0.09 km^3. This value of the reservoir volume is in agreement with values given in previous studies estimated through geochemical and geodetic data (Table 4), which range from 0.1 to 0.57 km^3 [*Albarède*, 1993; *Sigmarsson et al.*, 2005; *Peltier et al.*, 2008].

To refine our analysis of the system feeding the 2 January 2010 eruption, data from the continuous GPS network have been inverted using a simple Okada model in an elastic, homogeneous, and isotropic medium as defined above [*Okada*, 1985]. The Okada model is a good approximation of the usual magma injections geometry at Piton de la Fournaise, which typically occurs via dykes or sills [e.g., *Fukushima et al.*, 2005; *Peltier et al.*, 2008, 2009]. We used the nine stations located at that time on and around the central cone—the only ones having recorded significant ground displacements during the magma migration to the surface on 2 January 2010. Deformation recorded at the GPS stations was very weak for the remainder of the eruption. Postprocessing of the data was done using the GAMIT/GLOBK software, which take into consideration International GNSS Service (IGS) precise ephemeris, a stable support network of 20 IGS stations, a tested parameterization of the troposphere, and models of ocean loading, Earth, and Lunar tides. Mean horizontal and vertical accuracies are approximately 0.5 and 1 cm, respectively. Most of the ground deformation is located around the summit with a maximum of 9.7 cm recorded to the southeast of the eruptive fissure (Figure 13). The best fit model (74% of explained data) is shown on Figure 13, with a volume change equal to 0.33×10^6 m^3.

The volume of the dyke at the origin of the surface deformation recorded on 2 January 2010 is approximately 80% of the extruded volume observed at the surface during this period, after taking into account the average vesicularity of the magma. The height of the Okada source is 1200 m and its top is located at the average altitude of the GPS station of 2300 m, which gives a conduit length L from the reservoir to the summit of about 1400 m. This value is 82% of our first estimate of the conduit length made from seismic observations. If we propagate the range of possible values for the conduit length in equation (9), we obtain overpressure values between 3.7×10^6 Pa and 5.9×10^6 Pa, which in return gives from equation (11) a reservoir volume ranging from 0.25 km^3 to 0.54 km^3. The lack of strong deformation during the rest of the eruption suggests that, after the initial overpressure phase, the continuous supply of magma at the surface may have come from underlying storage zones and reached the vent through the already opened conduit.

7. Conclusions

Our observations suggest that the January 2010 eruption started with intense SO$_2$ degassing and several low-level lava fountains, with the highest reaching up to 30 m. The intense lava fountaining phase lasted for a day and a half and had a characteristic signature on the frequency content of the seismic tremor, with additional energy in the 3–5 Hz band in comparison to the rest of the eruption. The lava fountaining activity then decreased, going from seven active vents to only a single low-level lava fountain with a height of only 7 m, which progressively transformed into sporadic spattering and passive lava extrusion.

Photogrammetric reconstruction provide estimate of the average lava extrusion rate throughout the eruption, with values of 9.5 m^3 s^{-1} at the beginning of the eruption decreasing to 1.2 m^3 s^{-1} during the final phases. We compared lava extrusion rate to the infrasonic and seismic tremor energy and SO$_2$ emission rates. The temporal evolution of the seismic energy compares well with the time evolution of the extruded volume, suggesting a linear relationship between lava extrusion rate and seismic energy. We determined that for the January 2010 eruption, the rate of the seismic energy per second is linearly correlated to the lava extrusion rate. This relationship is supported by three eruptions that occurred during the 2009–2010 period. The total volume and average lava extrusion rate of these eruptions inferred from the associated seismic energy is in good agreement with values given in other studies. For these small-volume eruptions occurring close to the volcano summit, the lava extrusion rate is linearly proportional to 0.87 ± 0.11 times the seismic energy radiated per second. The linear relationship between the seismic energy and the lava extrusion rate, and the lack of correlation between the latter and the infrasonic signal, favors the assumption that the flow of the magma in the conduit is the main source of the volcanic tremor at Piton de la Fournaise. SO$_2$ flux is also a good proxy of average lava extrusion rate and provides values close to the ones estimated through photogrammetry. However, precise assessment of the time variation in plume height is critical to obtain robust estimate of lava extrusion rates from SO$_2$ flux measurements.

The relationship between seismic energy and lava extrusion rate allows us to evaluate the latter at a very high rate and thus provides important information on the dynamics of the 2 January 2010 eruption. Estimating the average lava extrusion rate during the initial lava fountaining phase allows us to infer the initial overpressure,

which is found to range from 3.7×10^6 Pa to 5.9×10^6 Pa, in good agreement with dyke propagation and eruption triggering models. We used a Mogi source model to constrain the volume of the shallow magma reservoir that supplied the 2 January 2010 eruption, based on our estimate of the initial overpressure, a geodetic model of the source causing the deformation recorded at the surface and the lava volume emitted during the initial phase inferred from the seismic energy. We found a reservoir volume between 0.25 km^3 and 0.54 km^3, which is in an good agreement with values provided by geochemical and geodetic data for other eruptions.

The multidisciplinary analysis presented in our study sheds light on crucial qualitative and quantitative relations between eruption dynamics, seismic and infrasonic signals, and especially on the direct link between the lava extrusion rate and the seismic energy of the volcanic tremor. If this relationship is confirmed for other eruptions, generalization of its use will lead to a better characterization, possibly continuously and in real time, of the temporal evolution of the eruptions that will occur at Piton de la Fournaise, as well as at other active basaltic volcanoes.

References

Albarède, F. (1993), Residence time analysis of geochemical fluctuations in volcanic series, *Geochim. Cosmochim. Acta*, *57*, 615–621.

Allard, P., J. Carbonnelle, N. Metrich, H. Loyer, and P. Zettwoog (1994), Sulfur output and magma degassing budget of Stromboli Volcano, *Nature*, *368*, 326–330.

Aki, K., and V. Ferrazzini (2000), Seismic monitoring and modeling of an active volcano for prediction, *J. Geophys. Res.*, *105*(B7), 16,617–16,640.

Aki, K., and R. Koyanagi (1981), Deep volcanic tremor and magma ascent mechanism under Kilauea, Hawaii, *J. Geophys. Res.*, *86*, 7095–7109.

Aki, K., and P. G. Richards (1980), *Quantitative Seismology*, vol. 1424, Freeman, San Francisco, Calif.

Aki, K., M. Fehler, and S. Das (1977), Source mechanism of volcanic tremor: Fluid driven crack models and their application to the 1963 Kilauea eruption, *J. Volcanol. Geotherm. Res.*, *2*, 259–287.

Andres, R. J., W. I. Rose, P. R. Kyle, S. deSilva, P. Francis, M. Gardeweg, and H. Moreno Roa (1991), Excessive sulfur dioxide emissions from Chilean volcanoes, *J. Volcanol. Geotherm. Res.*, *46*, 323–329.

Bachèlery, P. (1981), Le Piton de la Fournaise (Ile de la Réunion), Etude volcanologique, structurale et pétrologique, PhD thesis, Univ. Clermont-Ferrand II, France.

Baldi, P., M. Coltelli, M. Fabris, M. Marsella, and P. Tommasi (2008), High precision photogrammetry for monitoring the evolution of the NW flank of Stromboli volcano during and after the 2002–2003 eruption, *Bull. Volcanol.*, *70*(6), 703–715.

Batchelor, G. K. (1999), *An Introduction to Fluid Dynamics*, 634 pp., Cambridge Univ. Press, Cambridge.

Battaglia, J., K. Aki, and V. Ferrazzini (2005a), Location of tremor sources and estimation of lava output using tremor source amplitude on the Piton de la Fournaise volcano: 1. Location of tremor sources, *J. Volcanol. Geotherm. Res.*, *147*(3), 268–290.

Battaglia, J., K. Aki, and T. Staudacher (2005b), Location of tremor sources and estimation of lava output using tremor source amplitude on the Piton de la Fournaise volcano: 2. Estimation of lava output, *J. Volcanol. Geotherm. Res.*, *147*, 291–308.

Benoit, J. P., and S. R. McNutt (1997), New constraints on source processes of volcanic tremor at Arenal Volcano, Costa Rica, using broadband seismic data, *Geophys. Res. Lett.*, *24*(4), 449–452.

Brenguier, F., et al. (2012), First results from the Undervolc High resolution seismic and GPS network deployed on Piton de la Fournaise volcano, *Seismol. Res. Lett.*, *83*(1), 97–102.

Brenguier, F., N. M. Shapiro, M. Campillo, A. Nercessian, and V. Ferrazzini (2007), 3D surface wave tomography of the Piton de la Fournaise volcano using seismic noise correlations, *Geophys. Res. Lett.*, *34*, L02305, doi:10.1029/2006GL028586.

Bruce, P. M., and H. E. Huppert (1989), Thermal controls of basaltic fissure eruptions, *Nature*, *342*, 665–667.

Burton, M. R., et al. (2005), Etna 2004–2005: An archetype for geodynamically-controlled effusive eruptions, *Geophys. Res. Lett.*, *32*, L09303, doi:10.1029/2005GL022527.

Cayol, V., and F. H. Cornet (1998), Three dimensional modeling of the 1983–1984 eruption at Piton de la Fournaise volcano, Réunion Island, *J. Geophys. Res.*, *103*(B8), 18,025–18,037.

Chouet, B. A., G. De Luca, G. Milana, P. Dawson, M. Martini, and R. Scarpa (1998), Shallow velocity structure of Stromboli volcano, Italy, derived from small-aperture array measurements of Strombolian tremor, *Bull. Seismol. Soc. Am.*, *88*(3), 653–666.

Coppola, D., D. Piscopo, T. Staudacher, and C. Cigolini (2009), Lava discharge rate and effusive pattern at Piton de la Fournaise from MODIS data, *J. Volcanol. Geotherm. Res.*, *184*(1), 174–192.

Crampin, S. (1965), Higher modes of seismic surface waves: Second Rayleigh mode energy, *J. Geophys. Res.*, *70*(20), 5135–5143.

Deniel, C., G. Kieffer, and J. Lecointre (1992), New 230Th-238U and 14C age determinations from Piton des Neiges volcano, Réunion—A revised chronology for the differentiated series, *J. Volcanol. Geotherm. Res.*, *51*(3), 253–267.

Diefenbach, A. K., J. G. Crider, S. P. Schilling, and D. Dzurisin (2012), Rapid, low-cost photogrammetry to monitor volcanic eruptions: An example from Mount St. Helens, Washington, USA, *Bull. Volcanol.*, *74*(2), 579–587.

Diefenbach, A. K., K. F. Bull, R. L. Wessels, and R. G. McGimsey (2013), Photogrammetric monitoring of lava dome growth during the 2009 eruption of Redoubt Volcano, *J. Volcanol. Geotherm. Res.*, *259*, 308–316.

Di Muro, A., T. Staudacher, V. Ferrazzini, N. Métrich, P. Besson, B. Villemant, and K. Garofalo (2014), Shallow magma storage at Piton de la Fournaise volcano after 2007 summit caldera collapse tracked in Pele's hairs, in *Hawaiian Volcanoes: From Source to Surface*, *Geophys. Monogr. Ser.*, AGU, Washington, D. C.

Duncan, R. A. (1981), Hotspots in the Southern Oceans—An absolute frame of reference for motion of the Gondwana continents, *Tectonophysics*, *74*, 24–29.

Endo, E. T., and T. Murray (1991), Real-time seismic amplitude measurement (RSAM): A volcano monitoring and prediction tool, *Bull. Volcanol.*, *53*(7), 533–545.

Ferrazzini, V., and K. Aki (1992), Preliminary results from a field experiment on volcanic events at Kilauea using an array of digital seismographs, in *Volcanic Seismology*, edited by P. Gasparini, R. Scarpa, and K. Aki, pp. 168–189, Springer, Berlin.

Ferrazzini, V., K. Aki, and B. Chouet (1991), Characteristics of seismic waves composing Hawaiian volcanic tremor and gas piston events observed by a near source array, *J. Geophys. Res.*, *96*(B4), 6199–6209.

Fontaine, F. R., G. Roult, L. Michon, G. Barruol, and A. D. Muro (2014), The 2007 eruptions and caldera collapse of the Piton de la Fournaise volcano (La Réunion Island) from tilt analysis at a single very broadband seismic station, *Geophys. Res. Lett.*, *41*, 2803–2811, doi:10.1002/2014GL059691.

Fukushima, Y., V. Cayol, and P. Durand (2005), Finding realistic dike models from interferometric synthetic aperture radar data: The February 2000 eruption at Piton de la Fournaise, *J. Geophys. Res.*, *110*, B03206, doi:10.1029/2004JB003268.

Galle, B., M. Johansson, C. Rivera, Y. Zhang, M. Kihlman, C. Kern, and S. Hidalgo (2010), Network for Observation of Volcanic and Atmospheric Change (NOVAC)— A global network for volcanic gas monitoring: Network layout and instrument description, *J. Geophys. Res.*, *115*, D05304, doi:10.1029/2009JD011823.

Garofalo, K., T. Staudacher, V. Ferrazzini, P. Kowalski, P. Boissier, A. Dupont, A. Peltier, B. Villemant, and G. Boudon (2009), Eruptive SO$_2$-plume measurements at Piton de la Fournaise (Ile de la Réunion) by stationary NOVAC scanning MAX-DOAS instruments, EGU General Assembly, p. 12,113, Vienna, 19–24 April.

Giordano, D., A. Mangiacapra, M. Potuzak, J. K. Rusell, C. Romano, D. B. Dingwell, and A. Di Muro (2006), An expanded non-Arrhenian model for silicate melt viscosity: A treatment for metaluminous, peraluminous and peralkaline liquids, *Chem. Geol.*, *229*, 7117–7136.

Gordeev, E. I., V. A. Saltykov, V. I. Sinitsyn, and V. N. Chebrov (1990), Temporal and spatial characteristics of volcanic tremor wave fields, *J. Volcanol. Geotherm. Res.*, *40*(1), 89–101.

Harris, A. J., J. Dehn, and S. Calvari (2007), Lava effusion rate definition and measurement: A review, *Bull. Volcanol.*, *70*(1), 1–22.

Hibert, C., et al. (2014), Automated identification, location, and volume estimation of rockfalls at Piton de la Fournaise volcano, *J. Geophys. Res. Earth Surf.*, *119*, 1082–1105, doi:10.1002/2013JF002970.

Jaupart, C. (2000), Magma ascent at shallow levels, in *Sigurdsson*, edited by H. Houghton et al., pp. 237–245, Encyclopedia of Volcanoes, Academic Press.

Jaupart, C., and S. Vergniolle (1986), Separated two-phase flow and basaltic eruptions, *J. Geophys. Res.*, *92*, 13,715–13,719.

Jaupart, C., and S. Vergniolle (1988), Laboratory models of Hawaiian and Strombolian eruptions, *Nature*, *331*, 58–60.

Kazahaya, K., H. Shinohara, and G. Saito (1994), Excessive degassing of Izu-Oshima Volcano: Magma convection in a conduit, *Bull. Volcanol.*, *56*, 207–216.

Major, J. J., D. Dzurisin, S. P. Schilling, and M. P. Poland (2009), Monitoring lava-dome growth during the 2004-2008 Mount St. Helens, Washington, eruption using oblique terrestrial photography, *Earth Planet. Sci. Lett.*, *286*(1), 243–254.

Massin, F., V. Ferrazzini, P. Bachèlery, A. Nercessian, Z. Duputel, and T. Staudacher (2011), Structures and evolution of the plumbing system of Piton de la Fournaise volcano inferred from clustering of 2007 eruptive cycle seismicity, *J. Volcanol. Geotherm. Res.*, *202*(1-2), 96–106.

Métaxian, J. P., P. Lesage, and J. Dorel (1997), Permanent tremor of Masaya volcano, Nicaragua: Wave field analysis and source location, *J. Geophys. Res.*, *102*(B10), 22,529–22,545.

Michon, L., T. Staudacher, V. Ferrazzini, P. Bachèlery, and J. Marti (2007), April 2007 collapse of Piton de la Fournaise: A new example of caldera formation, *Geophys. Res. Lett.*, *34*, L21301, doi:10.1029/2007GL031248.

Michon, L., A. Di Muro, N. Villeneuve, C. Saint-Marc, P. Fadda, and F. Manta (2013), Eruptive activity of the summit cone of Piton de la Fournaise volcano (La Réunion island): A historical and geological review, *J. Volcanol. Geotherm. Res.*, *263*, 117–133.

Mogi, K. (1958), Relations between the eruptions of various volcanoes and the deformations of the ground surfaces around them, *Bull. Earthquake Res. Inst. Univ. Tokyo*, *36*, 99–134.

Murase, T., and A. R. McBirney (1973), Properties of some common igneous rocks and their melts at high temperatures, *Geol. Soc. Am. Bull.*, *84*(11), 3563–3592.

Nercessian, A., A. Hirn, J. C. Lépine, and M. Sapin (1996), Internal structure of Piton de la Fournaise volcano from seismic wave propagation and earthquake distribution, *J. Volcanol. Geotherm. Res.*, *70*(3), 123–143.

Okada, Y. (1985), Surface deformation due to shear and tensile faults in a half space, *Bull. Seismol. Soc. Am.*, *75*, 1135–1154.

Peltier, A., T. Staudacher, and P. Bachèlery (2007), Constraints on magma transfers and structures involved in the 2003 activity at Piton de La Fournaise from displacement data, *J. Geophys. Res.*, *112*, B03207, doi:10.1029/2006JB004379.

Peltier, A., V. Famin, P. Bachèlery, V. Cayol, Y. Fukushima, and T. Staudacher (2008), Cyclic magma storages and transfers at Piton de La Fournaise volcano (La Réunion hotspot) inferred from deformation and geochemical data, *Earth Planet. Sci. Lett.*, *270*(3), 180–188.

Peltier, A., P. Bachèlery, and T. Staudacher (2009), Magma transport and storage at Piton de La Fournaise (La Réunion) between 1972 and 2007: A review of geophysical and geochemical data, *J. Volcanol. Geotherm. Res.*, *184*(1), 93–108.

Pierce, A. D. (1989), *Infrasonics: An Introduction to its Physical Principles and Applications*, Infrasonical Soc. of Am., Melville, New York.

Prôno, E., J. Battaglia, V. Monteiller, J. L. Got, and V. Ferrazzini (2009), P-wave velocity structure of Piton de la Fournaise volcano deduced from seismic data recorded between 1996 and 1999, *J. Volcanol. Geotherm. Res.*, *184*(1), 49–62.

Proietti, C., M. Coltelli, M. Marsella, A. Sonnessa, and E. Bernardo (2008), Photogrammetric and lidar surveys on the Sciara del Fuoco to monitor the 2007 Stromboli eruption, *Proc. USEReST,* Napoli.

Roult, G., A. Peltier, B. Taisne, T. Staudacher, V. Ferrazzini, A. Di Muro, and the OVPF team (2012), A new comprehensive classification of the Piton de la Fournaise activity spanning the 1985-2010 period. Search and analysis of short-term precursors from a broad-band seismological station, *J. Volcanol. Geotherm. Res.*, *241–242*, 78–104, doi:10.1016/j.jvolgeores.2012.06.012.

Salerno, G. G., M. R. Burton, C. Oppenheimer, T. Caltabiano, D. Randazzo, N. Bruno, and V. Longo (2009), Three-years of SO$_2$ flux measurements of Mt. Etna using an automated UV scanner array: Comparison with conventional traverses and uncertainties in flux retrieval, *J. Volcanol. Geotherm. Res.*, *183*(1), 76–83.

Sigmarsson, O., M. Condomines, and P. Bachèlery (2005), Magma residence time beneath the Piton de la Fournaise volcano, Reunion Island, from U-series disequilibria, *Earth Planet. Sci. Lett.*, *234*, 223–234.

Staudacher, T. (2010), Field observations of the 2008 summit eruptions at Piton de la Fournaise (Ile de La Réunion) and implications on the 2007 Dolomieu collapse, *J. Volcanol. Geotherm. Res.*, *198*, 60–68.

Staudacher, T., V. Ferrazzini, A. Peltier, P. Kowalski, P. Boissier, P. Catherine, F. Lauret, and F. Massin (2009), The April 2007 eruption and Dolomieu crater collapse, two major events at Piton de la Fournaise (La Réunion Island), *J. Volcanol. Geotherm. Res.*, *184*, 126—137.

Stoiber, R. E., S. N. Williams, and B. J. Huebert (1986), Sulfur and halogen gases at Masaya caldera complex, Nicaragua: Total flux and variations with time, *J. Geophys. Res.*, *91*, 12,215–12,231.

Sutton, A. J., T. Elias, T. M. Gerlach, and J. B. Stokes (2001), Implications for eruptive processes as indicated by sulfur dioxide emissions from Kilauea Volcano, Hawaii, 1979–1997, *J. Volcanol. Geotherm. Res.*, *108*, 283–302.

Sutton, A. J., T. Elias, and J. Kauahikaua (2003), Lava-effusion rates for the Pu'u 'O'o-Kupaianaha eruption derived from SO$_2$ emissions and very low frequency (VLF) measurements, *U.S. Geol. Surv. Prof. Pap.*, *1676*, 137–148.

Taisne, B., F. Brenguier, N. M. Shapiro, and V. Ferrazzini (2011), Imaging the dynamics of magma propagation using radiated seismic intensity, *Geophys. Res. Lett.*, *38*, L04304, doi:10.1029/2010GL046068.

Vergniolle, S., and G. Brandeis (1996), Strombolian explosions: A large bubble breaking at the surface of a lava column as a source of sound, *J. Geophys. Res.*, *101*(B9), 20,433–20,448.

Vergniolle, S., and J. Caplan-Auerbach (2004), Infrasonic measurements of the 1999 basaltic eruption of Shishaldin volcano, Alaska: 2) Precursor to the Subplinian activity, *J. Volcanol. Geotherm. Res.*, *137*, 135–151.

Vergniolle, S., and C. Jaupart (1990), Dynamics of degassing at Kilauea volcano, Hawaii, *J. Geophys. Res.*, *95*(B3), 2793–2809.

Vergniolle, S., and M. Ripepe (2008), From Strombolian explosions to fire fountains at Etna Volcano (Italy): What do we learn from infrasonic measurements?, *Geol. Soc. London Spec. Publ.*, *307*(1), 103–124.

White, F. M. (1994), *Fluid Dynamics*, 736 pp., MacGraw Hill, New York.

Zlotnicki, J., J. C. Ruegg, P. Bachèlery, and P. A. Blum (1990), Eruptive mechanism on Piton de la Fournaise volcano associated with the December 4, 1983, and January 18, 1984 eruptions from ground deformation monitoring and photogrammetric surveys, *J. Volcanol. Geotherm. Res.*, *40*(3), 197–217.